COBEM 2021 26th International Congress of Mechanical Engineering
ABCM Associação Brasileira de Engenharia e Ciências Mecânicas
November 22-26, 2021, Virtual Congress, Brazil

COB-2021-1525
APPLICATION OF THE DOMAIN SUPERPOSITION TECHNIQUE TO STRESS ANALYSIS OF PLANE BENDING OF PLATES WITH CIRCULAR INCLUSIONS

J. S. Moraes[1]
L. O. C. Lara[2]
Mechanical Engineering Department, Federal University of Espírito Santo, Centro Tecnológico, Av. Fernando Ferrari, 540, Goiabeiras, 29075-910, Vitória, ES, Brazil
[1]jhonata.moraes@edu.ufes.br
[2]castrolara@hotmail.com

Abstract. *The Boundary Element Method faces difficulties to solve problems with non-homogeneous domains. This paper aims to analyze the stress distribution and concentration in piecewise homogeneous plates using the Domain Superposition Technique, a technique developed to solve problems with heterogeneous domains based on the sum of elastic energy retained in each distinct sector. Therefore, in order to demonstrate the robustness and adequacy of the technique to solve plane bending problems, three types of problems in seven different configurations were simulated. In the absence of analytical solutions, Finite Element Method solutions are used as reference for error evaluation.*

Keywords: *Boundary Element Method, Domain Superposition Technique, Piecewise Homogeneous Problems, Elastic Problems.*

1. INTRODUCTION

Materials with non-homogeneous properties, as composites, are widely used in many fields of engineering, such as aerospace, automotive, and chemistry. The effect of heterogeneities in the material can lead to concentrate local stress and, ultimately, result in fracture and failure of the materials or structures. Therefore, much attention has been paid by many researchers to stress concentration problems in composite materials or structures (Mao and Xu, 2013).

Evaluating the distribution of stresses in non-homogeneous domains using analytical methods is generally unfeasible due to its complexity. Although experimental recent works have been carried out evaluating the stress concentration near inclusions (Misseroni *et al.*, 2014), experimental solutions are expensive due to the necessity of specific and expensive machines. Thus, numerical methods are generally used to analyze this type of problems and, among the various discrete methods that have been used for the evaluation of stress distribution, the Finite Element Method (FEM) is the most used for non-homogeneous properties.

Dispite the Boundary Elements Method (BEM) is a reference for the other methods when solving differential equations which it is possible to reduce the domain mesh to a boundary mesh (Cheng and Cheng, 2005), the modeling of physically non-homogeneous problems is one of its less suitable applications. Considering that heterogeneity is located by sector, it is possible to use the sub-regions technique, a procedure based on domain partition. (Brebbia, 1984). Although the technique is efficient for simpler analysis, as problems become more complex, the addition of many internal contours increases the computational cost, decreases the accuracy of the results and requires more elaborate programming.

In this context, recent works (Loeffler and Mansur, 2016; Lara *et al.*, 2018) using Boundary Element Method have been carried out to develop an alternative methodology to solve heterogeneous problems, called Domain Superposition Technique (DST). Conceptually, the proposed technique differs widely from the classical technique of division of the domain into sub-regions since it is based on the sum of elastic energy retained in each different sector, capable of computing changes in constitutive properties and thus simulating both sector heterogeneities and inclusions within the domain, in a very simple and effective way.

Loeffler and Mansur (2016) explain that the proposed technique models the complete domain constituted by sectorial homogeneities superposing sub-domains with different properties to a homogeneous complete domain. Furthermore, influence coefficients are used to link all sectors, which are given in non-homogeneous boundary by integration with the

source points located in the complete or surrounding domain.

This work aims to apply the domain superposition technique to analyze the stress distribution in plates with circular inclusions subject to plane bending, as shown in Fig. 1. Three types of examples of elastic problems with non homogeneous domain, with seven different inclusion configurations, are simulated using this alternative methodology. The results obtained by the BEM are compared to the FEM as a reference.

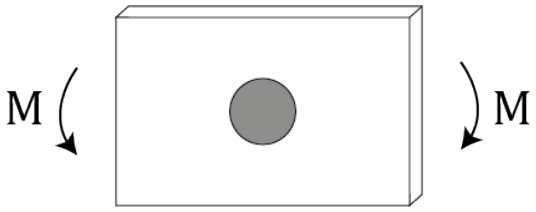

Figure 1. Plate with circular inclusion subjected to plane bending.

2. THE DOMAIN SUPERPOSITION TECHNIQUE

Considering a 2-D linear elastic problem, continuous, with isotropic properties, in static condition and without body forces, Navier's Equation governs this type of problem (Timoshenko, 1970). Although, it is convenient writing the equation using Lamé parameters λ and μ (Boresi *et al.*, 2010):

$$\mu u_{j,ii}(\mathbf{X}) + (\lambda + \mu) u_{i,ij}(\mathbf{X}) = 0 \tag{1}$$

In Eq. 1, vector $u_i(\mathbf{X})$ represents displacements field in "i" direction and $\mathbf{X}$ represents a point with coordinates (x_1,x_2). The index notation $u_{j,ii}$ represents the application of the Laplace operator, and $u_{i,ij} = \nabla(\nabla \cdot u) = grad(div(u))$.

Integrating Eq. 1 in a Ω domain with a Γ boundary and applying the method of weighted residuals using the Kelvin fundamental solution $u_j^*(\xi; \mathbf{X})$ as auxiliary function, which considers a source point $\xi \in \Omega$ where all load, flow or action is concentrated (Brebbia, 1984), the following integral equation can be written:

$$\mu \int_\Omega u_{j,ii}(\mathbf{X}) u_j^*(\xi; \mathbf{X}) d\Omega(\mathbf{X}) + (\lambda + \mu) \int_\Omega u_{j,ii}(\mathbf{X}) u_j^*(\xi; \mathbf{X}) d\Omega(\mathbf{X}) = 0 \tag{2}$$

Without loss of generality, a piecewise homogeneous domain is defined as shown in Fig. 2. It consists of an external domain Ω^e, with properties μ^e and λ^e and an internal domain Ω^i, with properties μ^i and λ^i.

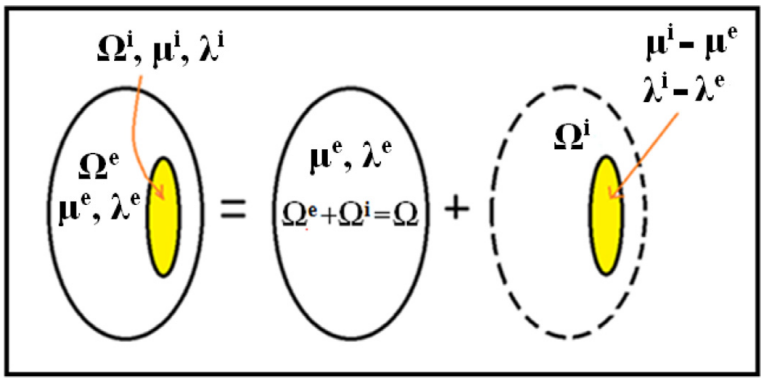

Figure 2. Complete and sectorial domains with homogeneous properties.

In each domain the properties are constants. A complete or surrounding domain is elected, such as shown, with homogeneous properties, and the other sub-domains are correlated with it. Thus, applying superposition, Eq. 2 can be rewritten as:

$$\mu^e \int_{\Omega^e} u_j^e(\mathbf{X})_{ii} u_j^*(\xi;\mathbf{X}) d\Omega^e(\mathbf{X}) + (\lambda^e + \mu^e) \int_{\Omega^e} u_i^e(\mathbf{X})_{ij} u_j^*(\xi;\mathbf{X}) d\Omega^e(\mathbf{X}) + \mu^i \int_{\Omega^i} u_j^i(\mathbf{X})_{,ii}\, u_j^*(\xi;\mathbf{X}) d\Omega^i(\mathbf{X}) + \left(\lambda^i + \mu^i\right) \int_{\Omega^i} u_i^i(\mathbf{X})_{ij} u_j^*(\xi;\mathbf{X}) d\Omega^i(\mathbf{X}) = 0 \tag{3}$$

The kernel of integrals is considered to be composed of integrable functions. Assuming $\lambda^i = \lambda^e + \lambda^*$ and $\mu^i = \mu^e + \mu^*$, the following equation is achieved in terms of the complete and the surrounding domain:

$$\mu^e \int_{\Omega} u_j^e(\mathbf{X})_{,ii} u_j^*(\xi;\mathbf{X}) d\Omega^e(\mathbf{X}) + (\lambda^e + \mu^e) \int_{\Omega} u_i^e(\mathbf{X})_{ij} u_j^*(\xi;\mathbf{X}) d\Omega^e(\mathbf{X}) + \mu^* \int_{\Omega^i} u_j^i(\mathbf{X})_{ji} u_j^*(\xi;\mathbf{X}) d\Omega^i(\mathbf{X}) + (\lambda^* + \mu^*) \int_{\Omega^i} u_i^i(\mathbf{X})_{ij} u_j^*(\xi;\mathbf{X}) d\Omega^i(\mathbf{X}) = 0 \tag{4}$$

Eq. 4 represents the main objective of DST: analyze a heterogeneous problem as a superposition of a contribution related to a background homogeneous domain and other sectors, also homogeneous. This contribution is given in terms of balance of elastic energy.

2.1 Boundary Equations

The equations needed for numerical implementation are provided by reaching the inverse form of the integral equation, applying the Divergence Theorem (Brebbia, 1984; Katsikadelis, 2002). Thus, after manipulating the equation and applying the divergence theorem, Eq 4 can be rewritten as:

$$\mu^e \left[-P_j u_j(\xi) + \int_{\Gamma} p_j(\mathbf{X}) u_j^*(\xi;X) d\Gamma(\mathbf{X}) - \int_{\Gamma} p_j^*(\xi;\mathbf{X}) u_j(\mathbf{X}) d\Gamma(\mathbf{X}) \right] + \mu^* \left[-P_j u_j^i(\xi) + \int_{\Gamma^i} p_j^i(\mathbf{X}) u_j^*(\xi;\mathbf{X}) d\Gamma^i(\mathbf{X}) - \int_{\Gamma^i} p_j^*(\xi;\mathbf{X}) u_j^i(\mathbf{X}) d\Gamma^i(\mathbf{X}) \right] = 0 \tag{5}$$

Where Γ represents the domain boundaries, which can be divided into inner and outer boundary Γ^i and Γ^e, respectively, P_j are the tractions.

It is convenient to adopt a dyadic structure to the fundamental solution and its traction derivative, respectively $u_j^*(\xi;X)$ and $p_j^*(\xi;\mathbf{X})$ (Lara *et al.*, 2018). They represent displacement and tractions in "j" direction and "$\mathbf{X}$" point of domain due to a unit load acting in "i" direction at source point "ξ". Besides, it is also introduced a dyadic coefficient C_{ij} taking into account the position of the source point (within or outside domain, or on the boundary). Then inverse boundary integral equations turns into:

$$\mu^e \left[-C_{ij}(\xi) u_j(\xi) + \int_{\Gamma} p_j(\mathbf{X}) u_{ij}^*(\xi;\mathbf{X}) d\Gamma(\mathbf{X}) - \int_{\Gamma} u_j(\mathbf{X}) p_{ij}^*(\xi;\mathbf{X}) d\Gamma(\mathbf{X}) \right] + \mu^* \left[-C_{ij}^i(\xi) u_j^i(\xi) + \int_{\Gamma^i} p_j^i(\mathbf{X}) u_{ij}^*(\xi;\mathbf{X}) d\Gamma^i(\mathbf{X}) - \int_{\Gamma^i} u_j^i(\mathbf{X}) p_{ij}^*(\xi;\mathbf{X}) d\Gamma^i(\mathbf{X}) \right] = 0 \tag{6}$$

Where u_{ij}^* and p_{ij}^* are the aforementioned fundamental Kelvin solutions. In terms of the material properties G and ν, the Dirac function δ and the Euclidean distance r between X and ξ, fundamental solutions are presented by Brebbia (1984):

$$u_{ij}^* = \frac{1}{8\pi G(1-v)} \left[(3-4v) \ln\left(\frac{1}{r}\right) \delta_{ij} + r_{,i} r_{,j} \right] \tag{7}$$

$$p_{ij}^* = \frac{-1}{4\pi G(1-v) r} \left[\frac{\partial r}{\partial n} \left((1-2v)\delta_{ij} + 2r_{,j} r_{,i} \right) - (1-2v) \left(r_{,i} r_{,j} - r_{,j} r_{,i} \right) \right] \tag{8}$$

Lara *et al.* (2018) also explains that the inverse integral equation can be interpreted as a equilibrium between elastic energy stored and the work done by applied tractions. However, Loeffler and Mansur (2016) justify that the internal sector

energy can be computed only by the elastic energy given in terms of the displacement values u_j^i at internal source points. So the equation can be simplified:

$$\left[-C_{ij}(\xi)u_j(\xi) + \int_\Gamma p_j(\mathbf{X})u_{ij}^*(\xi;\mathbf{X})d\Gamma(\mathbf{X}) - \int_\Gamma u_j(\mathbf{X})p_{ij}^*(\xi;\mathbf{X})d\Gamma(\mathbf{X})\right] = +\frac{\mu^*}{\mu^e}\left[\int_{\Gamma^i} u_j^i(\mathbf{X})p_{ij}^*(\xi;\mathbf{X})d\Gamma^i(\mathbf{X})\right] \tag{9}$$

3. NUMERICAL SIMULATIONS

Three types examples of plane bending are solved using the Domain Superposition Technique, disconsidering body forces. To validate results obtained by DST, results obtained by the Finite Element Method were considered.

The main geometry of the problems, as well as the boundary condition are shown in Fig 3. The external domain is kept the same for all configurations, that is, only the number of inclusions and their positions are changed.

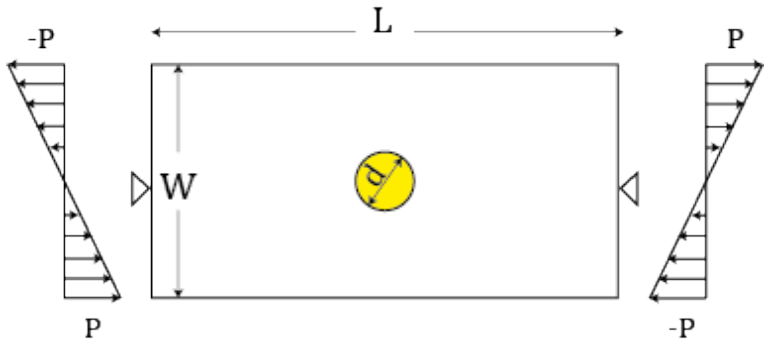

Figure 3. Main geometry and boundary conditions of problems.

The center nodes of the side boundaries are kept fixed in the X and Y directions, and an uniformly varying load is applied to the sides of the plate to simulate the plane bending effect. The numerical simulations considers $W = 6$, $L = 12$, $d = 1.5$ and $P = 1.2$.

3.1 First Example

The first simulation consists of analyzing the interaction of multiple separate inclusions with same properties in plane bending of plates. Three configurations as shown in Fig. 4 were evaluated.

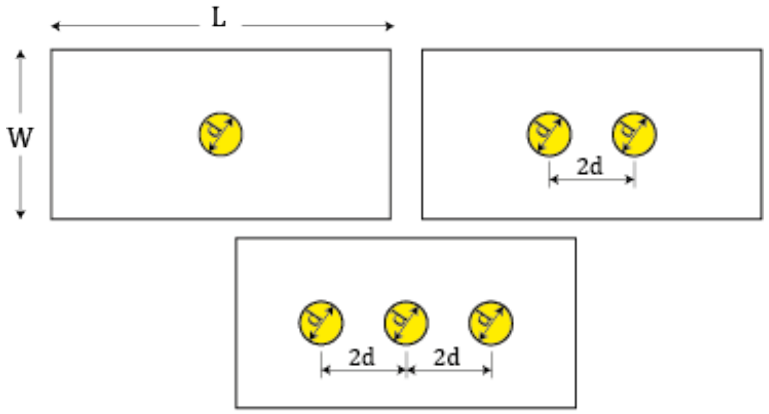

Figure 4. Three configurations evaluated in first example.

For the first configuration, three meshes were simulated: 36 elements + 24 sectorial elements, 72 elements + 24 sectorial elements and 144 + 76 sectorial elements. The results were compared with a 7292 elements FEM mesh. The property $\mu_1 = 1$ is associated with the plate, while μ_2 associated with the inclusions, varies. Figure 5 presents results of normal stress in X direction in the horizontal line $y = 6$, top boundary of plate.

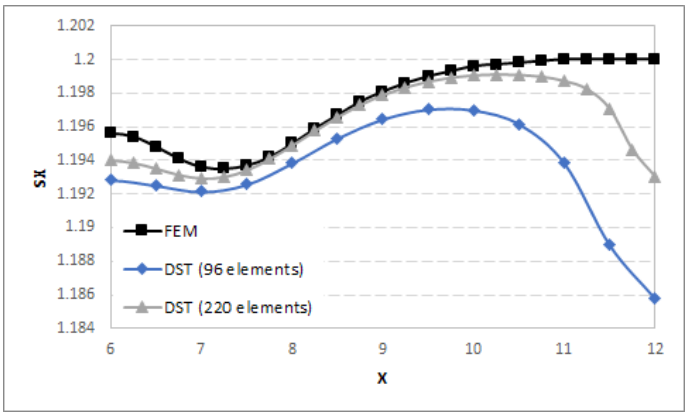

Figure 5. Value of normal stress in x direction along the horizontal line for different meshes for $\mu_2 = 10$ of first configuration.

Mesh results for 36 + 24 elements were not plotted in Fig. 5 due to its associated to high error, as shown in Fig. 6. After the mesh refinement, the results reached an average error of 0.1% compared to the results obtained by the FEM.

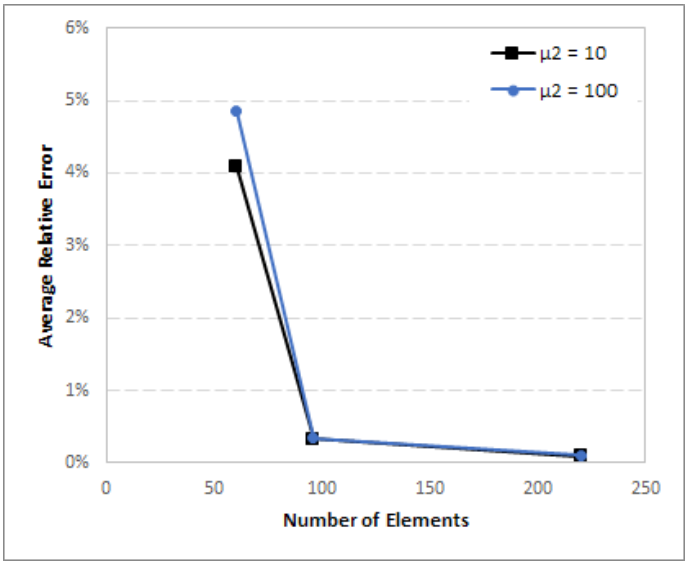

Figure 6. Comparison of mean and maximum errors for normal stresses in X direction along the horizontal line $y = 6$ for $\mu_2 = 10$ and $\mu_2 = 100$.

According to Fig. 6, it is also possible to infer from the error results that as μ_2 from 10 to 100, the associated error also increases for meshes with few discrete elements. As the number of elements increases, this error variation between $\mu_2 = 10$ and $\mu_2 = 100$ is not noticeable.

For the second configuration, two meshes were simulated with 144 and 296 elements. DST results were compared to a 7424 elements FEM mesh and results were also obtained along horizontal line at $y = 6$, top boundary of plate. The results obtained are shown in Fig. 7. In agreement with the previous configuration, results close to $x = 12$ have greater relative error. However, for 296 elements, FEM and DST present the same behavior.

For third configuration, only one mesh with 180 elements were simulated due to the high fidelity of results already obtained with this single mesh. As with the other configurations, DST results were compared to a 7599 elements FEM mesh and results were also obtained along horizontal line at $y = 6$, top boundary of plate. The results obtained are shown in Fig. 8.

As presented above, once again DST and FEM results agree with each other, resulting in an average relative error of 0.3%, as shown in the Fig. 8 by the dotted line.

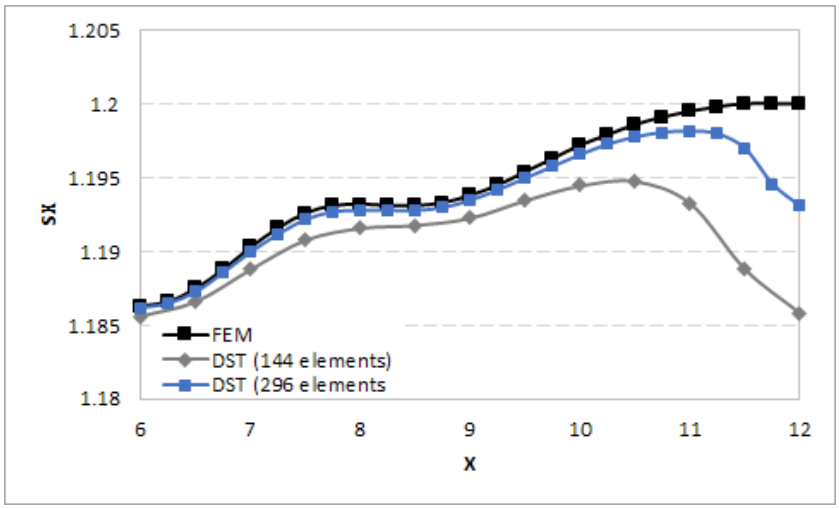

Figure 7. Value of normal stress in x direction along the horizontal line for different meshes for $\mu_2 = 10$ of second configuration.

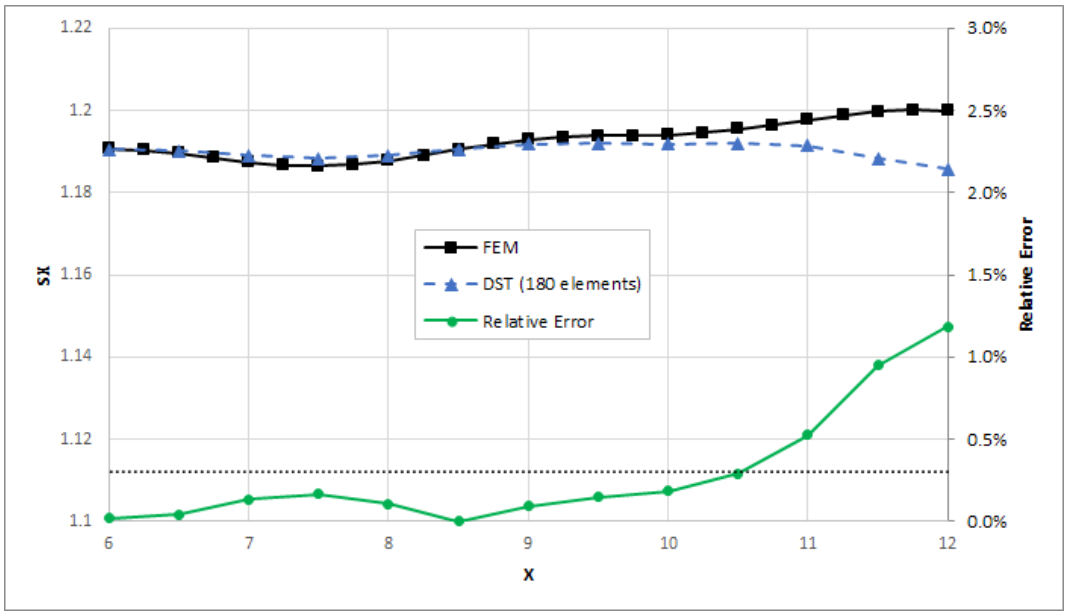

Figure 8. On the primary axis (left), values of normal stress in x direction along the horizontal line for different meshes for $\mu_2 = 10$ of third configuration. On the secondary axis (right), relative error.

Finally, the different interactions on the plate are shown in Fig. 9. Since the modulus of elasticity is greater in the inclusions, the stress at remote points, such as the horizontal line $y = 6$, ends up decreasing, as the displacements for a given load also decrease.

3.2 Second Example

The second simulation consists of analyzing the interaction of multiple separate inclusions with different properties in plane bending of plates. Two configurations were evaluated, as shown in Fig. 10

For both plates, the external domain was discretized into 144 elements. For the first configuration, 288 elements were used in total, while for the second configuration 252 elements were used. The results obtained for both plates are shown in Fig. 11 and Fig. 12. Both results are compared with the results of the previous example, where all inclusions have sector property $\mu = 10$, in order to understand the stress distortion behavior by inserting an inclusion with ten times stiffer elasticity property.

As shown above, the comparison between DST and FEM shows that both curves are similar disregarding the regions near the edges. The comparison on the right shows the effect of inserting an inclusion with different properties.

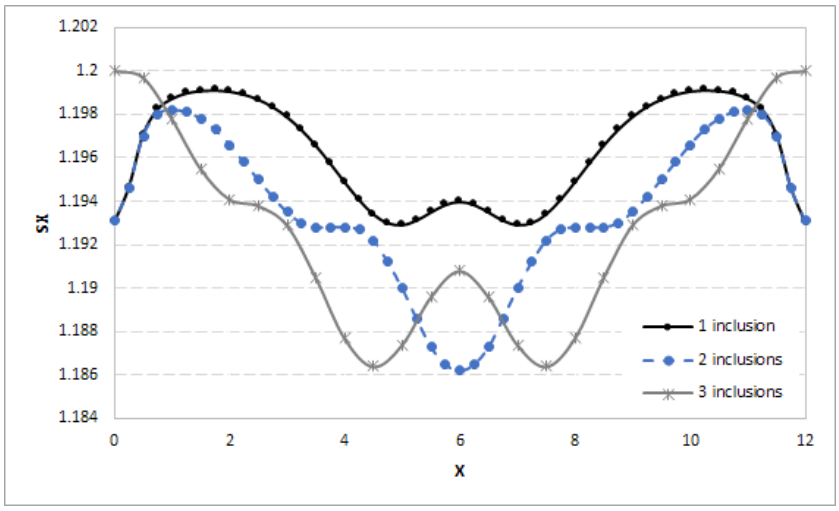

Figure 9. Normal stress in X direction behavior due to interactions between inclusions.

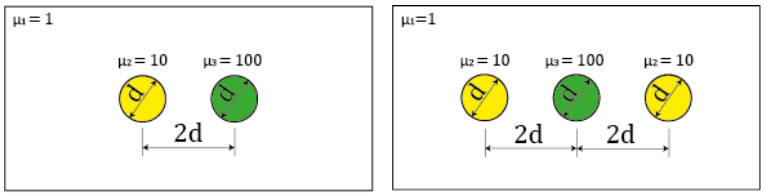

Figure 10. Two configurations evaluated in second example.

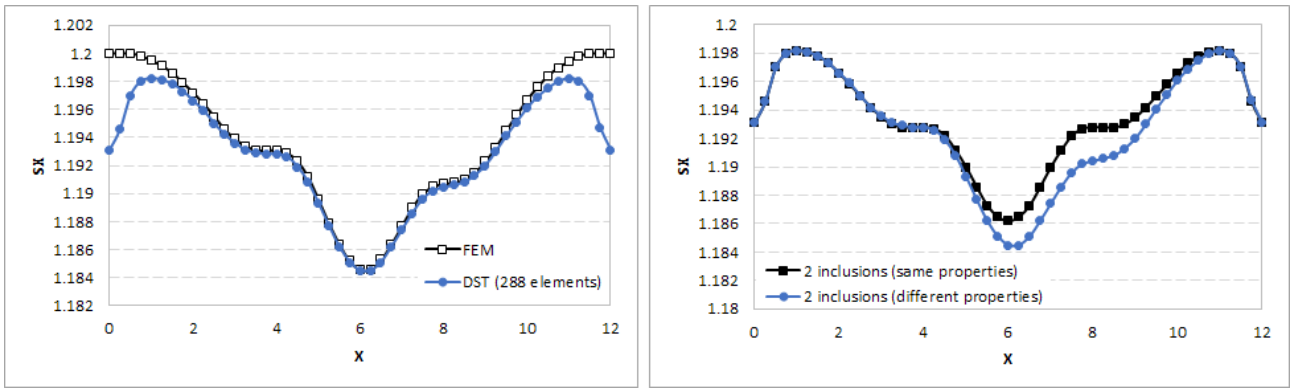

Figure 11. On the left, values of normal stress in X direction along horizontal line $y = 6$ for $\mu_2 = 10$ and $\mu_3 = 100$ on first configuration. On the right, comparison of 2 inclusions with same properties and different properties.

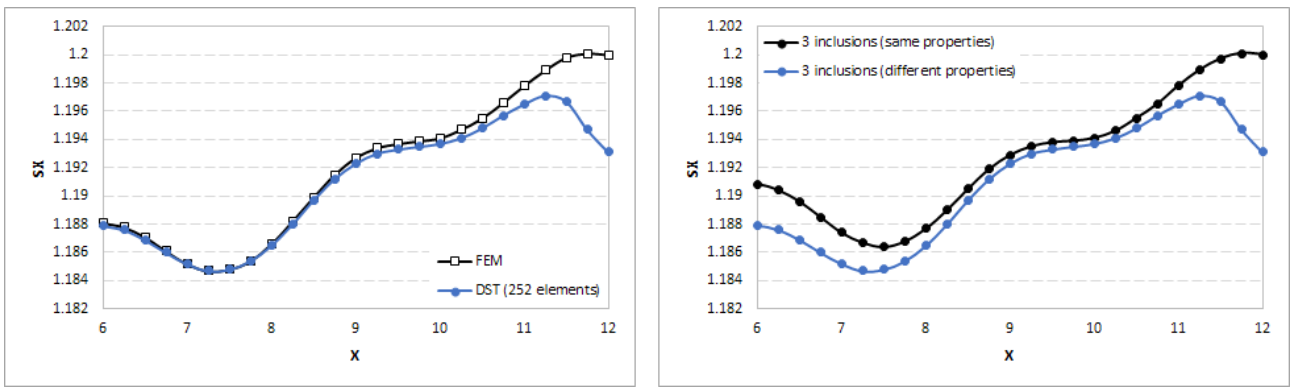

Figure 12. On the left, values of normal stress in X direction along horizontal line $y = 6$ for $\mu_2 = 10$ and $\mu_3 = 100$ on second configuration. On the right, comparison of 3 inclusions with same properties and different properties.

For the first configuration, both curves fit well from x = 0 to x = 4, approximately. After this value of x, the other inclusion affects the stress results, decreasing them since your $\mu_3 > \mu_2$. For the second one, both curves are sightly different. In fact, there is a sudden change in the modulus of elasticity between the inclusions, distorting the stress field for both sides and interfering with the stress field close to the other inclusions, causing the difference between the curves presented.

3.3 Third Example

The objective of third simulation is to analyze the interaction of one inclusion within another. Two configurations were evaluated, as shown in Fig. 13

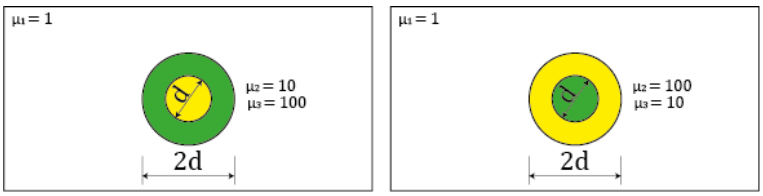

Figure 13. Two configurations evaluated in third example.

For the second example, only the last (408 elements) was used. The results obtained for both plates are shown in Fig. 14.

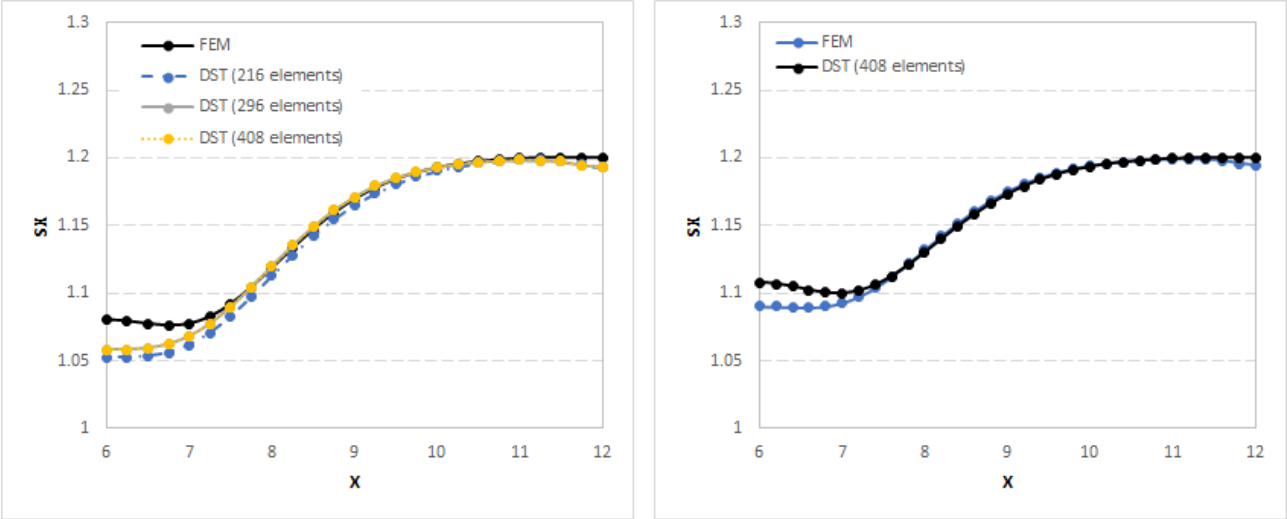

Figure 14. Two configurations evaluated in third example.

About first configuration, the graph shows that the results obtained with the DST are close enough outside the range between $x = 4$ and $x = 8$. For the 296 and 408 meshes there is no difference in the results. Mean error is shown in Fig. 15, demonstrating good accuracy even to coarse mesh.

4. CONCLUSIONS

According to the results of examples, the Domain Superposition Technique proves to be a powerful technique for stress analysis of non-homogeneous domains. Even though few examples have been tested using the technique so far, it is possible that this technique can be applied to more complex problems, such as Elastoplastic and Fracture Mechanics problems.

The technique has high precision, even with not so refined meshes, being an advantage compared to domain methods. In addition, the technique is shown to be highly reproducible, since to implement the model, new matrices similar to the classical matrix H are created.

5. ACKNOWLEDGEMENTS

This research was supported by the National Council for Scientific and Technological Development - CNPq - Brazil.

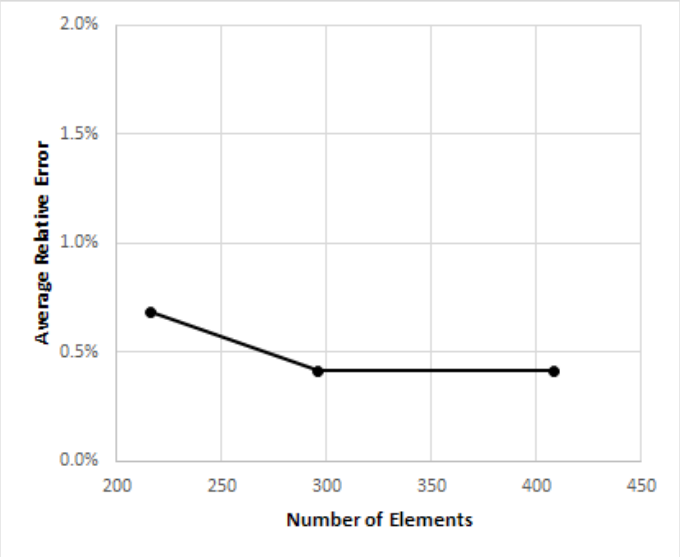

Figure 15. Mean error in first configuration for different mashes.

6. REFERENCES

Boresi, A.P., Chong, K. and Lee, J.D., 2010. *Elasticity in engineering mechanics*. John Wiley & Sons.

Brebbia, C., 1984. "Boundary element techniques". *Theory and Applications in Engineering*, pp. 451–454.

Cheng, A.H.D. and Cheng, D.T., 2005. "Heritage and early history of the boundary element method". *Engineering Analysis with Boundary Elements*, Vol. 29, No. 3, pp. 268–302. ISSN 0955-7997. doi:https://doi.org/10.1016/j.enganabound.2004.12.001. URL https://www.sciencedirect.com/science/article/pii/S0955799705000020.

Katsikadelis, J.T., 2002. *Boundary elements: theory and applications*. Elsevier.

Lara, L., Loeffler, C., Barbosa, J. and Mansur, W., 2018. "The technique of domain superposition to solve piecewise homogeneous elastic problems". *Engineering Analysis with Boundary Elements*, Vol. 94, pp. 1–9. ISSN 0955-7997. doi:https://doi.org/10.1016/j.enganabound.2018.05.009. URL https://www.sciencedirect.com/science/article/pii/S0955799717306471.

Loeffler, C.F. and Mansur, W.J., 2016. "Sub-regions without subdomain partition with boundary elements". *Engineering Analysis with Boundary Elements*, Vol. 71, pp. 169–173. ISSN 0955-7997. doi:https://doi.org/10.1016/j.enganabound.2016.07.018. URL https://www.sciencedirect.com/science/article/pii/S0955799716301862.

Mao, C. and Xu, X., 2013. "Bending problem of a finite composite laminated plate weakened by multiple elliptical holes". *Acta Mechanica Solida Sinica*, Vol. 26, No. 4, pp. 419–426. ISSN 0894-9166. doi:https://doi.org/10.1016/S0894-9166(13)60037-3. URL https://www.sciencedirect.com/science/article/pii/S0894916613600373.

Misseroni, D., Dal Corso, F., Shahzad, S. and Bigoni, D., 2014. "Stress concentration near stiff inclusions: Validation of rigid inclusion model and boundary layers by means of photoelasticity". *Engineering Fracture Mechanics*, Vol. 121-122, pp. 87–97. ISSN 0013-7944. doi:https://doi.org/10.1016/j.engfracmech.2014.03.004. URL https://www.sciencedirect.com/science/article/pii/S001379441400071X.

Timoshenko, S., 1970. "Goodier. jn, theory of elasticity". *New. York McGraw—Hil1*, Vol. 970, No. 4, pp. 279–291.

7. RESPONSIBILITY NOTICE

The authors are solely responsible for the printed material included in this paper.